TURBULENT DRAG REDUCTION BY SPANWISE WALL OSCILLATIONS

D. Zhou*

Department of Mechanical Engineering, California State University
Sacramento, CA 95819, U.S.A.
zhoud@ecs.csus.edu

K. S. Ball

Department of Mechanical Engineering, Virginia Polytechnic Institute and State University
Blacksburg, VA 24061, U.S.A
ball@vt.edu

*Corresponding Author

Abstract   The objective of this paper is to examine the effectiveness of wall oscillation as a control scheme of drag reduction. Two flow configurations are considered: constant flow rate and constant mean pressure gradient. The Navier-Stokes equations are solved using Fourier-Chebyshev spectral methods and the oscillation in sinusoidal form is enforced on the walls through boundary conditions for the spanwise and streamwise (for the case of inclination cycle) velocity components. Results include the effects of oscillation frequency, amplitude, oscillation orientation and peak wall speed on drag reduction at a Reynolds number of 180 based on wall-shear velocity and channel half-width as well as the Reynolds number dependency in both flow configurations. Drag reduction as a function of peak wall speed is compared with both experimental and numerical data and the agreement is good in the trend and in the quantity. Comparison between these two flow configurations in the transient response to the sudden start of wall oscillation, turbulence statistics and instantaneous flow fields is detailed and differences are clearly shown. This analysis and comparison have allowed some light to be shed on the way that oscillations interact with wall turbulence.

Keywords   Turbulence, Drag Reduction, Spanwise Wall Oscillation

چکیده   هدف از ارائه این مقاله، امتحان تاثیر پذیری نوسان دیواره به عنوان طرحی برای کاهش نیــروی مقــاوم است. دو شکل نمایش جریان لحاظ شده است؛ آهنگ ثابت جریان و میانگین ثابت گرادیان فشار معادلات ناویه استوکس با بکار بردن روش های طیفی "فوریه چبیشو" حل شــده انــد و نوســانات بــه شــکل سینوســی از روی شرایط مرزی برای مولفه های عرضی و طولی سرعت به دیواره ها اعمال شده است (برای حالت چرخه عکــس العملی یا بر هم کنشی). نتایج، شامل آثار فرکانس نوسان، دامنه، جهت نوسان و اوج سرعت سیال روی دیــواره، بر کاهش نیروی مقاومت در عدد رنولدز ۱۸۰ مبتنی بر ســرعت بــرش دیــواره و نــیم پهنــای کانــال و همچنــین وابستگی عدد رنولدز در هر دو شکل نمایش جریان است. کــاهش نیــروی مقاومــت بــه عنــوان نیــروی تــابعی ازپیشینه سرعت سیال روی دیواره با هر کدام از داده های تجربی و عددی مقایسه شــده اســت. تطــابق کیفــی و کمی خوبی به چشم می‌خورد. مقایسه بین این دو شکل نمایش جریان در پاسخ گذرا به شروع ناگهــانی نوســان دیواره، آمار تلاطم و میدان های آنی جریان به تفصیل انجام شده و تفاوت ها بــه وضــوح بیــان شــده انــد. ایــن تحلیل و مقایسه، روزنه امیدی برای پیدا کردن راه حل برای شرایطی که تلاطم و نوسانات دیواره بر هــم کــنش دارند، بوجود می‌آورد.

1. INTRODUCTION

In the early 1990s, Akhavan and co-workers [1] proposed a simple active control technique. In this technique, oscillating the wall along the spanwise direction in a turbulent boundary layer flow leads to a sustained turbulent drag reduction [1]. DNS studies performed for a turbulent channel flow showed that up to 40 % skin-friction drag reduction was possible at appropriate oscillation

parameters. Their results were confirmed by the subsequent DNS of [2-5]. Experimental investigations conducted by [6-12] have confirmed and extended the DNS results. The possibility of turbulent flow control by wall oscillation has also been extended to a turbulent pipe flow by [8] in an experimental study and by [13] using DNS. With similar control principles, a control scheme using a spanwise traveling wave has drawn more attention recently. Numerical simulations performed by [14,15] showed that more than 30 % drag reduction can be achieved.

It is generally accepted that well-organized turbulence structures exist which play a key role in the dynamics of turbulent boundary layers [16]. The two most prominent structural features of near-wall turbulence are low- and high-speed "streaks," and quasi-streamwise vortices, roughly aligned in the streamwise direction. It is also recognized that there is a close correlation between the near-wall streamwise vortices and the high skin-friction observed in turbulent boundary layers [17]. The exact relationship, though, is still an active area of research. On one hand, the streamwise vortices are associated with both ejections and sweeps, which are major contributors to the Reynolds shear stress in the wall region [18,19]. The sweep motion owing to a strong streamwise vortex is believed to create a region of high skin-friction on the wall [20,21]. On the other hand, the streaks are generated by nearby streamwise vortices through the lifting of low-speed fluid near the wall. That is, the characteristic elongation of streaks is the passage of streamwise vortices due to advection which leaves the lifted low-speed fluid underneath them in their wake [16]. The streaks soon become unstable after being created and they break up into a chaotic motion. This process is also believed to be accompanied by a rapid increase of skin-friction at the wall and thus streamwise vortices are also responsible for the increase in skin-friction during the formation of the streaks [22]. The streamwise vortices are mainly found in the buffer region ($y^+=10\sim50$) [23] and their genesis and evolution are a self-sustaining process which involves the wall-layer streaks through an instability-based mechanism [24]. If the formation of streamwise vortices is greatly suppressed, a boundary control scheme would be expected to lead to a significant reduction in the skin-friction drag.

The mechanism by which the wall oscillation results in a drag reduction has been investigated by previous workers. This topic was also discussed by [25-27] and [3]. More recently [28] has reviewed the potential physical mechanisms responsible for the turbulent drag reduction by transverse motions, including wall oscillations. Most of the proposed drag reduction mechanisms, even though they differ greatly in appearance, involve a lateral shift of the streamwise vortices, which in turn disrupt the low-speed-streaks' formation and homogenize the near-wall layer. From experimental observations [10] argued that it is the near-wall fluid and streaks which are shifted laterally, rather than the streamwise vortices above the wall. Like the self-sustaining process of turbulence, the underlying physics is not yet fully explained.

Direct numerical simulation has the advantage of providing much detailed information from which insight into physics of turbulence can be gained [29]. For a turbulent flow between two infinite parallel plates, two types of formulations can be applied, corresponding to either a fixed instantaneous mass flow rate or a constant mean pressure gradient in the streamwise direction. These two flows are characterized by different Reynolds numbers, Re_Q for constant flow rate and Re_P for constant pressure gradient. The differences between these two flow configurations have been discussed by [30,31]. For a plane channel flow at its equilibrium, results produced with both problem formulations are identical. Later on, in the present paper, it will be seen that, when the wall oscillation is applied to the two flow configurations, both flows will experience a transient process before they reach their own new equilibrium states, which presents different behaviors from each other. Therefore, it is worthwhile to examine and compare the flow features between both flow configurations.

With the intent to shed some light on the drag reduction mechanism, a scheme of wall oscillation has been tested in a plane turbulent channel with two flow configurations: constant flow rate and constant pressure gradient, under the same Reynolds number. The wall oscillation takes the sinusoidal form and the oscillation frequency, amplitude and direction are considered. The results

are compared with previous experimental and numerical data when possible. A cost-and-benefit comparison is presented to assess the practical application of this technique. The DNS of turbulent channel flow with three different Reynolds numbers, Re_τ = 180, 125 and 100, is also conducted to investigate the dependency of the Reynolds number. Finally, turbulence statistics and flow structures are presented to illustrate the key features in the flow with wall oscillation and the physical mechanisms responsible for the turbulent drag reduction.

2. NUMERICAL METHODS

The fully developed turbulent channel flow is studied in the rectangular coordinates as shown in Figure1. Direct numerical simulation of three-dimensional, time-dependent continuity and momentum equations has been performed for low Re turbulent channel flow to determine the effectiveness of wall oscillation. Standard periodic boundary conditions in the streamwise and spanwise directions are imposed and the no-slip condition is enforced at the channel walls such that the wall movement is considered directly through the boundary conditions of spanwise and streamwise (if inclined) velocity components. To solve the governing equations at each time step, pseudospectral methods, Fourier series in the streamwise and spanwise directions and Chebyshev polynomial expansions in the wall-normal direction [32], are used for spatial derivatives. The time advancement is made by a semi-implicit method: the Crank-Nicolson scheme
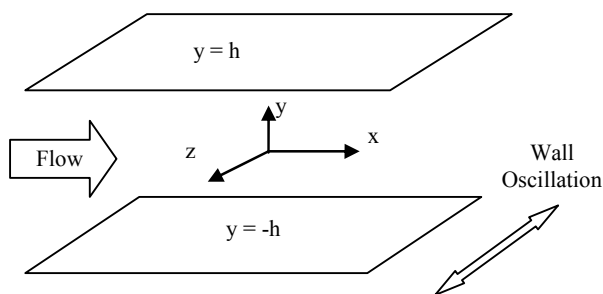
for viscous terms and the Adams-Bashforth method for the nonlinear terms [23]. More details can be found in [5] and [33].

The simulations are conducted with two flow configurations:

- A fixed mass flow rate where the mean pressure gradient varies with time;
- A constant pressure gradient where the flow rate varies with time.

The computational box is chosen to be 4πh, 2h and 2πh in the streamwise, wall-normal and spanwise directions, respectively. Most numerical computations are performed at Re_τ = 180 using grids of (64×129×64) in the (streamwise, wall-normal, spanwise) directions. The simulation with the most effective wall oscillation is repeated using finer grids of (128×129×128) at the same Reynolds number to obtain turbulence statistics and instantaneous flow fields. Detailed information about the effect of grids on numerical solutions can be found in [5]. This Reynolds number, the periodic box and the spatial resolution chosen by [23] are used in the present base flow for comparison. Two other Reynolds numbers, Re_τ = 100 and 125, are also tested to study the Reynolds number dependency using the same computational domain of (4πh×2h×2πh) and grids of (64×129×64) as with Re_τ = 180 simulations.

Before the oscillation control is applied, all simulations are allowed to develop until the turbulent flow fields reach a statistical equilibrium. The size of the time advancement step is around $0.072\nu/u_\tau^2$. Once the velocity field reaches the statistically stationary state the governing equations are integrated further in time to obtain time averages of the various statistical quantities. The total averaging time is about $8000\nu/u_\tau^2$, which is about 55 wash-out times [34]. For consistency, all the wall units are referenced with respect to the unperturbed conditions throughout the paper.

Figure 1. Coordinate system and geometry in a channel.

3. TRANSIENT PROCESS AND DRAG REDUCTION

An initial run was carried out at Re_τ = 180 with the oscillation imposed by moving both channel

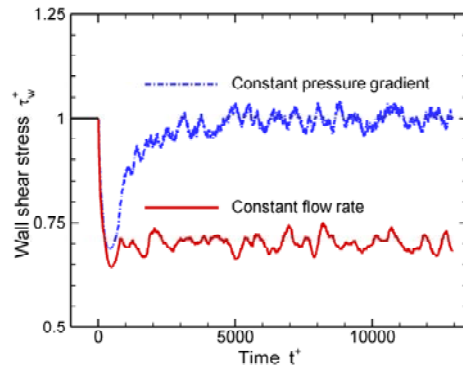walls at a spanwise velocity, $W_{wall} = 0.8(Q/2h)\sin(2\pi ft)$, as suggested by [1]. Here, Q is the volumetric flow rate per unit width in the streamwise direction. The oscillation frequency f^+ is set to be 0.01, corresponding to $T^+_{osci} = 100$ considered by [1] and the oscillation velocity amplitude of 0.8Q/2h corresponds to a value of 12.48 in wall units. The time histories of the streamwise wall-shear stresses for both flow configurations are subject to the same start of wall oscillation and are plotted in Figure 2a. It shows that the wall-shear stress for both flow configurations drop sharply at the same rate within the time $t^+ < 500$. As time marches on, the wall-shear stress in the fixed mass flow fluctuates about a reduced value, while the flow driven by a constant pressure gradient adjusts itself to reach a new two-dimensional equilibrium state, characterized by an increase in the flow rate as shown in Figure 2b. This can be explained by the momentum balance as follows. If a control surface is defined to be that which encloses the entire computational domain, a simple momentum balance in streamwise direction results in the following equation:

$$\frac{\partial Q}{\partial t} = -\frac{2h}{\rho}\left(\frac{dP}{dx}\right) + \frac{2\tau_w}{\rho} \qquad (1)$$
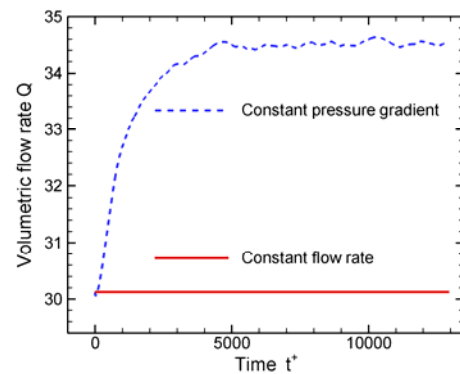
This equation shows that the wall-shear stress at each moment is balanced by the mean pressure gradient that is required to drive a fixed mass flow. However, in order to maintain the mean pressure gradient unchanged, the mass flow rate has to be increased to compensate for the reduced wall-shear stress. Note that the velocity gradient at wall (and thus the wall-shear stress) is reduced by the wall oscillation at a constant flow rate whereas both the velocity gradient at the wall and the wall-shear stress stay constant with a constant pressure gradient.

Since there is no pressure (form) drag in the plane channel flow, the skin-friction drag reduction in a fixed mass flow is naturally quantified by the change either in the wall-shear stress or in the mean pressure gradient. Thus, the drag reduction percentage is defined as

$$\text{Drag reduction \%} = (\tau_{w_0} - \tau_{w_{osci}})/\tau_{w_0} \qquad (2\text{-}1)$$

(a)

(b)

Figure 2. (a) Time evolution of the streamwise wall-shear stress subsequent to the start of wall oscillation and (b) Time evolution of the streamwise flow rate subsequent to the start of wall oscillation.

$$\text{Drag reduction \%} = [(\frac{dP}{dx})_0 - (\frac{dP}{dx})_{osci}]/(\frac{dP}{dx})_0 \qquad (2\text{-}2)$$

Here, the subscript '0' in Equations 2 represents the value for the stationary-wall channel flow and 'osci' for the oscillating-wall channel flow. For the constant pressure gradient flow, since both wall-shear stress and pressure gradient remain the same before and after the control at their equilibrium states, Equations 2 are no longer appropriate to define the drag reduction percentage. The only option seems to be to use the flow rate. According to [35], the skin-friction coefficient is related to the Reynolds number by an empirical relation:

$$C_f = 0.073\,\text{Re}_m^{-1/4} \qquad (3)$$

Where the friction coefficient is $C_f = \tau_w / (\rho U^2 / 2)$ and the Reynolds number is $Re_m = 2hU / \nu$. If the volumetric flow rate is defined as $Q = 2hU$, by substituting (3) into (2-1), the formula is finally obtained to calculate the drag reduction percentage in a constant pressure gradient flow as

$$\text{Drag reduction \%} = (Q_{osci}^{7/4} - Q_0^{7/4}) / Q_0^{7/4} \qquad (4)$$

For the oscillation parameters tested here, 29.9 % drag reduction is obtained for the fixed mass flow and 27.2 % for the constant pressure gradient flow. The small difference in drag reduction between these two flow configurations might be attributed to the difference in the Reynolds number. In the case with a fixed flow rate, Re is decreased from 180 to about 162 by the wall oscillation whereas Re_m (= 5600) remains the same. In the case with a fixed pressure gradient, Re_m is increased from 5600 to about 6176 the by wall oscillation whereas Re_τ (= 180) remains the same. Thus, in the constant pressure gradient case, the drag reduction gained is at a higher corresponding Reynolds number Re_τ, which leads to less drag reduction as discussed in the study of Reynolds number dependency.

Having demonstrated that the drag reduction can be achieved for both flow configurations, the effects of various oscillation parameters on the drag reduction will be examined.

4. EFFECTIVENESS OF DRAG REDUCTION

4.1. Frequency and Amplitude The extent of drag reduction depends primarily on the frequency and amplitude of the wall oscillations. In the numerical simulations, the wall oscillation is imposed through the boundary conditions for the spanwise velocity component as discussed above, that is:

$$W_{wall} = W_a \sin(2\pi ft) \qquad (5)$$

Where W_a is the velocity amplitude calculated from the channel flow rate. In experiments, on the

other hand, the motion of wall surfaces directly corresponds to the spanwise displacement of the oscillating walls:

$$z_{wall} = (\frac{\Delta z}{2})\sin(2\pi ft) \qquad (6)$$

Here, Δz is the peak-to-peak amplitude in the spanwise direction within one oscillation period. Thus, there are two ways to perform the parametric study: the first way is to fix the velocity amplitude W_a and vary the frequency f, or vice versa; the second way is to fix the peak-to-peak amplitude Δz and change the frequency f, or vice versa. In order to apply the second way and compare with the experimental results, Equation 6 is modified by multiplying $2\pi f$ on both sides of the equation and the yield of boundary conditions for the spanwise velocity in numerical simulations is:

$$W_{wall} = W_p \sin(2\pi ft) \qquad (7)$$

Where $W_{wall} = (z_{wall})(2\pi f)$ and $W_p = (\Delta z / 2)(2\pi f)$, which is also termed the peak wall speed. Computations are then made for various combinations of frequency and velocity amplitude which are listed in Table 1. At the fixed frequency f, the velocity amplitude W_a are varied and preset the computed results in Figure 3. Then the same results are collected by fixing W_a while varying f and finally present the results in Figure 4.

At each frequency, as shown in Figure 3 for both flow configurations, larger velocity amplitudes lead to a greater amount of drag reduction and the trend is monotonic. It is also observed from Figure 3 that a maximum drag reduction has not been achieved. Figure 4 illustrates the variation of drag reduction with frequencies at various fixed values of velocity amplitude and an optimal oscillation frequency appears to exist for fixed velocity amplitudes. The maximum drag reduction is found around $f^+ = 0.02$ for the constant pressure gradient flow as shown in Figure 4a, while Figure 4b shows that the largest drag reduction for the constant mass flow is obtained around $f^+ = 0.01$, which is the same value as [1].

The difference in the optimal frequency for both flow configurations seems closely related to the

TABLE 1. Oscillation Frequency and Amplitude.

f^+	$W_a / (Q/2h)$	W_a^+
0.005	0.25	3.9
	5.0	7.8
	0.8	12.48
	1.0	15.56
0.010	0.25	3.9
	5.0	7.8
	0.8	12.48
	1.0	15.56
0.020	0.25	3.9
	5.0	7.8
	0.8	12.48
	1.0	15.56
0.040	0.25	3.9
	5.0	7.8
	0.8	12.48
	1.0	15.56

Figure 3. Variation of drag reduction with velocity amplitude.

change in flow structures caused by the wall motion. If a flat plate is oscillated in a stationary fluid, because of the viscous diffusion from the plate surface, a thin boundary layer of shear flow (also called Stokes layer) is formed over the plate. When the spanwise wall oscillation is imposed on the boundary layer flow, the high-shear-layer regions on the wall are gradually moved to the interior of the channel through the Stokes layer. The thickness of Stokes layer δ can be related to the oscillation frequency roughly by the following correlation, $\delta^+ = \sqrt{4\pi/f^+}$ [2]. As presented later in the present paper, one major change in turbulence statistics by a wall oscillation is the outward shift of peak values for the turbulent intensity and production away from the wall, suggesting a thickened boundary layer. The bigger shift of peak values for the turbulent intensity and production is found in the fixed mass flow, indicating a thicker boundary layer in the oscillating channel. Since the oscillation effect is supposed to be felt toward the edge of the boundary layer, a bigger δ^+ is required to reac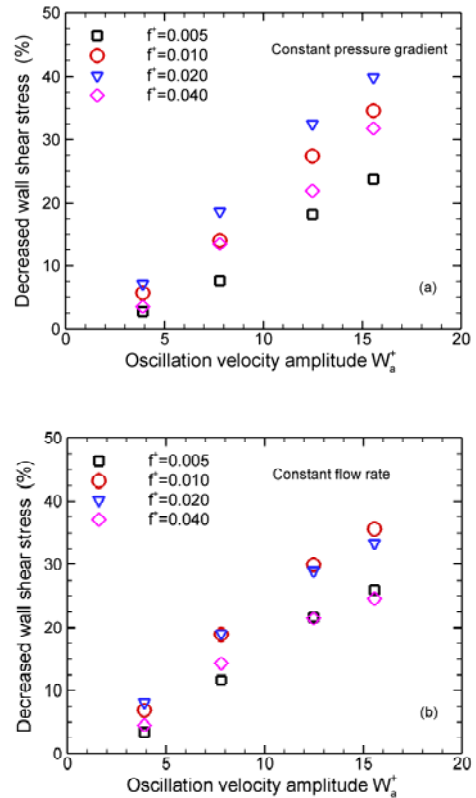h the thickened boundary layer edge to achieve a maximum oscillation effect. As a result, a smaller f^+ (= 0.01) is needed to generate the bigger δ^+ in the fixed mass flow to achieve the maximum effect, while in the constant pressure gradient flow, a bigger f^+ (= 0.02) is required to generate the smaller δ^+ which corresponds to the less thickened boundary layer, in order to gain the maximum benefit of a wall oscillation.

4.2. Oscillation Orientation   Since the potential physical mechanism by which the wall oscillation results in a drag reduction involving the lateral shift of the streamwise vortices, which in turn disrupt the low-speed streak formation, an attempt is made to intensify the relative displacement of the near-wall streaks and the streamwise vortices above by dragging the channel wall obliquely with respect to the streamwise direction. The inclination angle γ is set to be 0˚, 30˚, 60˚ and 90˚, with γ = 0˚

corresponding to the streamwise oscillation and $\gamma = 90°$ corresponding to the spanwise oscillation. Numerical experiments are performed at the oscillation frequency of $f^+ = 0.01$ combined with the velocity amplitude of $W_a^+ = 12.48$. Computed results for both flow configurations plotted in Figure 5 show that only the spanwise wall oscillation ($\gamma = 90°$) has achieved the maximum drag reduction whereas the streamwise oscillation ($\gamma = 0°$) leads to the least gain. This finding is consistent with what was found by [36] in their active control study. They found that a U-control scheme was also less effective than a W-control scheme to reduce the drag, where U refers to the streamwise direction and W to the spanwise direction when blowing or suction is applied on the channel wall. Similar results were also reported by [37]. Further examination shows, however, there does appear to be a break-point near $\gamma = 60°$ where the drag reduction reaches nearly the maximum amount with very little additional gains as γ approaches $90°$. Since the spanwise oscillation appear to be the most effective at $\gamma = 90°$ in the turbulent channel flow configuration studied here no further attempt was made to study other wall oscillation configurations.

4.3. Peak Wall Speed Since the amount of the drag reduction depends on both frequency and peak-to-peak amplitude in experiments [9] suggested that the amount of drag reduction due to a spanwise wall oscillation would better correlate with the peak wall speed W_p, which is defined in Equation 7. This suggestion was confirmed by [7] and later by [11] in their experimental studies. This seems to be the case in the present study. Computations are first made by fixing the frequency f while varying the peak-to-peak amplitude Δz which determines peak wall speed W_p. Then the same computed results are collected and presented in Figure 6 as a function of peak wall speed. The oscillation frequency f^+ tested is set to be 0.007, 0.1, 0.014, 0.021 and 0.028, respectively and the peak-to-peak amplitude Δz^+ is chosen to be 120, 240, 360, 480, 720 and 765, respectively. Figure 6 shows, when the drag reduction is plotted as a function of the peak wall speed for both flow configurations, the data correlate well, with a sharp increase of drag
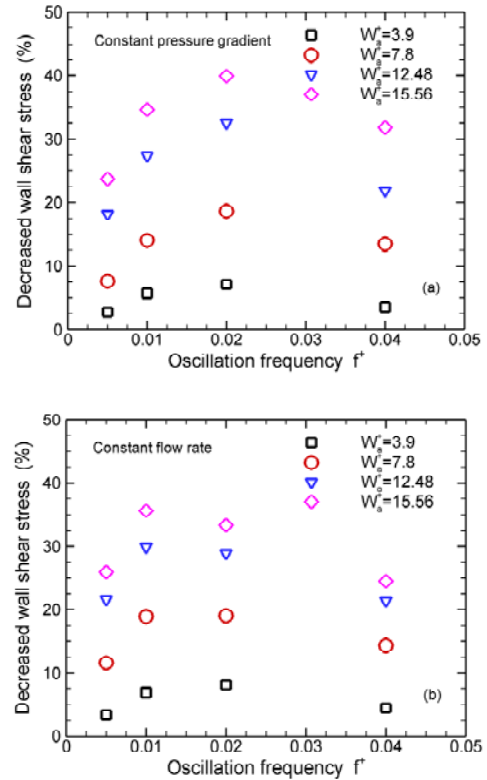

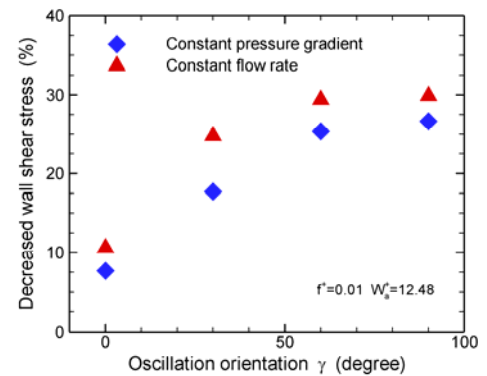**Figure 4**. Variation of drag reduction with oscillation frequency.

Figure 5. Variation of drag reduction with oscillation orientation.

reduction initially. The increase in drag reduction stops after $Wp^+ = 20$ for a fixed mass flow. At a constant pressure gradient, the amount of drag

reduction keeps increasing even after $Wp^+ = 70$. Although over 80 % drag reduction is possible for an appropriate combination of frequency and amplitude, the flow has been relaminarized at such a big drag reduction [33].

Results from previous researchers as well as those from the present simulation at a fixed mass flow are shown in Figure 7. It shows that, initially the amount of drag reduction increases rapidly with the peak wall speed and then the profile levels out after $Wp^+ = 20$. This trend appears to follow Wu's data although the maximum drag reduction is about 42 % for the present data but is 30 % for his data. The difference in drag reduction may be attributed to the Reynolds number difference which will be discussed next.

4.4. Reynolds Number During the effectiveness study of a drag reduction, the Reynolds number is the only dynamic parameter required to be investigated besides the oscillation parameters themselves. Trujillo [11] had conducted experiments to study the effect of Reynolds number on the drag reduction and the Reynolds number ranged from $Re_\theta = 500$, 950, 1400, to $Re_\theta = 2400$, based on the momentum thickness. It was observed and concluded in his thesis that within the range of these Reynolds numbers the amount of drag reduction that could be achieved is independent of the Reynolds number. In order to examine the dependency of the present numerical results of drag reduction at the lower Reynolds number range, further computations are conducted at $Re_\tau = 125$ and 100 with the same combinations of the oscillation frequency and velocity amplitude as $Re_\tau = 180$ simulations. The effects of frequency and amplitude for lower Reynolds numbers are similar to those at $Re_\tau = 180$ [5]. Figure 8 depicts representative cases for the dependency of drag reduction upon the Reynolds number. Drag reduction is observed to become smaller as the Reynolds number is increased. Such an observation is also consistent with the findings published by [3].

Based upon the numerical investigations of [3], this researcher's and the experimental results of [11], it is speculated that, at the lower Reynolds numbers, the amount of drag reduction will depend on the Reynolds number. In particular, drag reduction decreases with the increasing of the
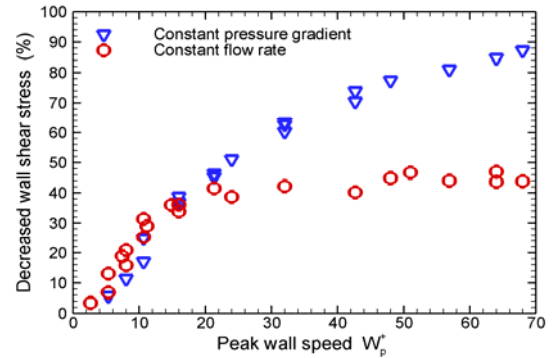

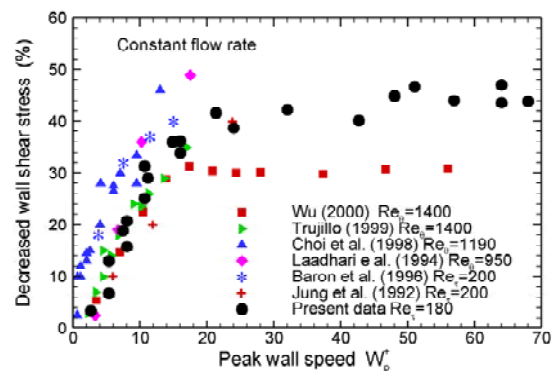**Figure 6**. Drag reduction as a function of peak wall speed.

Figure 7. Drag reduction as a function of peak wall speed, present results compared to literature.
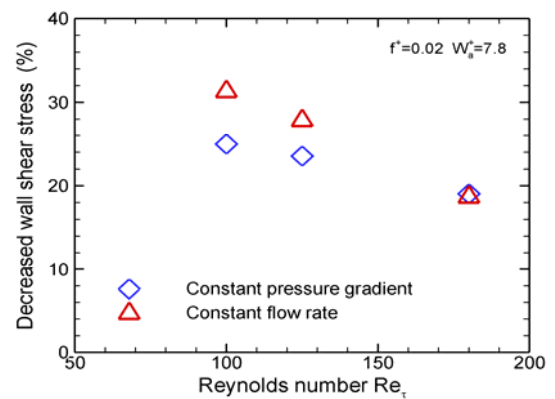

Figure 8. Dependency of drag reduction on reynolds number.

Reynolds number and beyond a certain threshold Reynolds number, the amount of drag reduction

remains unchanged with further increases in the Reynolds number. The exact threshold Reynolds number will not be pursued in the present study, but will be left to a future investigation.

4.5. Cost and Benefit From a practical point of view, the cost of a drag reduction technique should be considered. In the present work using wall oscillations, the power saved is simply defined as

$$\text{Power Saving} = (\tau_{w_0} - \tau_{w_{osci}}) \bullet U \qquad (8)$$

Here, $\tau_{w_{osci}}$ and τ_{w_0}, respectively, represent the streamwise wall shear stress in the oscillating-wall channel and in the stationary-wall channel and U is the bulk velocity in the streamwise direction. Without any other practical costs included, the power cost in an ideal situation is defined as

$$\text{Power} \qquad \text{Cost} \qquad = \\ \frac{1}{t_{tot}} \int_0^{t_{tot}} \left\langle \tau_{wz_{osci}}(x_2 = \pm h, t) \bullet W_{wall}(t) \right\rangle dt \qquad (9)$$

Here, $\tau_{wz_{osci}}$ represents the spanwise wall shear stress in the moving-wall channel. The benefit obtained would be the difference between the power input and the power output. These definitions are similar to those utilized by [2].

Besides, it was found from the above parametric study that, when the wall oscillation is imposed in the spanwise direction, the larger amplitude of velocity oscillation results in further drag reduction at an optimal oscillation frequency. Therefore, the oscillation frequency is set to be the optimal value of $f^+ = 0.01$ for the fixed mass flow and $f^+ = 0.02$ for the fixed pressure gradient flow, while the amplitude of the velocity oscillation varies from $W_a /(Q/2h) = 0.25, 0.5, 0.8$, to 1.0. Computations are then made at a Reynolds number of $Re_\tau = 180$. The computed cost and benefit, normalized by the streamwise friction power ($\tau_{w_0} \bullet U$) in the stationary-wall channel are summarized in Table 2.

The data in Table 2 clearly show that for both configurations a net benefit is obtained only at the lower velocity amplitude of 0.25Q/2h and beyond that, further gains are achieved at a substantial penalty. This result is consistent with the published data of [2] and also similar to the observation found by [10] in his cost/benefit comparison for a family of wall oscillation frequencies at the fixed peak-to-peak amplitude. Despite the large magnitude of drag reduction, the spanwise wall oscillation does not seem to be economically practical for the turbulent flow configurations studied, in which the entire wall is put into motion. However, better results may be possible with other configurations of wall oscillation on turbulent flows, in which the cost of the wall motion may be reduced.

TABLE 2. A Cost and Benefit Comparison.

Constant Pressure Gradient: $f^+ = 0.02$				
$W_a/(Q/2h)$	0.25	0.5	0.8	1.0
Saving	17.1%	28.6%	41.3%	49.9%
Cost	13.8%	55.3%	142 %	222 %
Net Benefit	+ 3.3%	-26.7%	-100 %	-172 %
Constant Flow Rate: $f^+ = 0.01$				
$W_a/(Q/2h)$	0.25	0.5	0.8	1.0
Saving	13.9%	25.9%	36.2%	42.6%
Cost	9.6%	38.0%	98.7%	154%
Net Benefit	+ 4.3%	-12.1%	-62.5%	- 111%

5. TURBULENCE STATISTICS

Some key features of the flow field obtained from the wall oscillations were examined for both flow formulations and also compared with those in the stationary channel. Finer grids of ($128 \times 129 \times 128$) were used for the detailed analysis of the modified flow fields. The computational parameters were set at $Re_\tau = 180$, $f^+ = 0.01$ and $W_a^+ = 12.48$. The statistically steady state of the oscillating channel flow was identified by the linear profile of the total shear stress. It should be kept in mind that at a constant flow rate, the velocity gradient at the wall is reduced by the wall oscillation but it stays constant at a constant pressure gradient.

5.1. Mean Properties Mean velocity profiles, normalized by the wall-shear velocity of the unperturbed flow, are plotted in Figure 9 with a wall coordinate and in Figure 10 with a global coordinate. Figures 9a and 10a show that, in the case of a constant pressure gradient, the slope of the mean velocity profile near the oscillating wall remains the same as that of the stationary channel, resulting in the wall-shear stress unchanged before and after the wall control. The slope of the log-law profile, however, is appreciably increased in the oscillating channel. This upward shift in log-law has previously been observed in drag-reduced flows such as riblets [20] and is considered to be a result of the increase in the viscous sublayer thickness. In addition, the increased flow rate is clearly reflected in the mean velocity profile of Figure 10a.

Figure 9b shows that, for the fixed mass flow, the profiles of the mean velocity in an oscillating channel are found to deviate from the standard law of the wall when they are scaled by the wall-shear velocity of stationary channel and they would show the usual upward shift in the logarithmic region if normalized by the actual wall-shear velocity of an oscillating channel [5]. Figure 10b
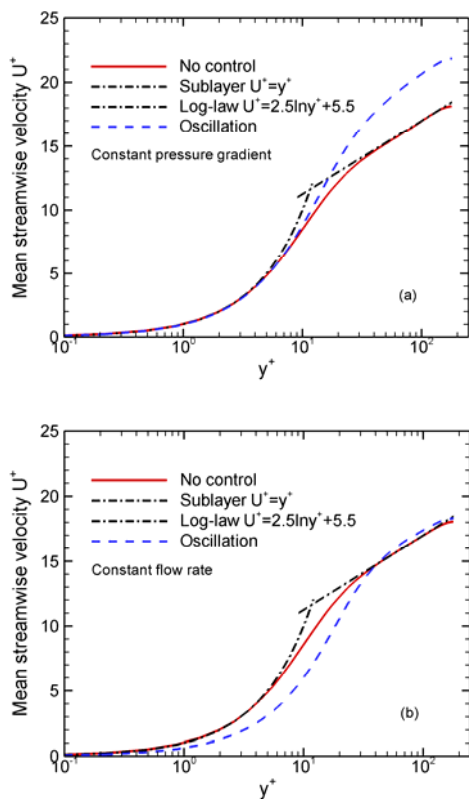

Figure 9. Mean velocity profiles in wall coordinate: (a) Constant pressure gradient, (b) Constant flow rate.
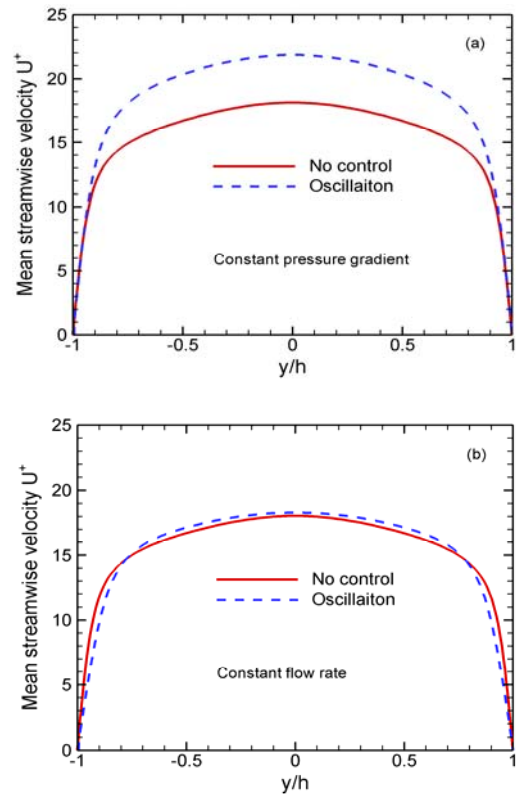

Figure 10. Effect of addition of H_2O_2 on (a) Cobalt and (b) Manganese concentration after 10 minutes leaching with different acid concentrations.

shows the mean velocity is reduced by the wall oscillation through the wall region up to $y/h \approx 0.8$, while further away from the wall the mean velocity is slightly increased in order to conserve the mass.

5.2. Reynolds Shear Stress The Reynolds shear stress and the total Reynolds shear stress are shown in Figure 11. Total shear stresses are straight lines, indicating that each flow has reached an equilibrium state. Note that the total shear stress in Figure 11b has been normalized by local variables for the oscillating channel. In the case of a constant pressure gradient, there is a noticeable reduction in the Reynolds shear stress, but mainly confined to the near-wall region. Comparatively, the reduction in Reynolds shear stress for the fixed mass flow is substantial and throughout the channel.

5.3. Turbulence Intensities In the case of a constant pressure gradient, the turbulence intensities are plotted in Figure 12 and compared

with those above the stationary wall. Figure 12a shows that the streamwise turbulence intensity is reduced by the wall motion, with a 15 % drop in the maximum value. The wall-normal turbulence intensity in Figure 12b is found basically unchanged in the near-wall region but slightly decreased in the magnitude for the rest of the channel. The spanwise turbulence intensity in Figure 12c is found to increase primarily near the
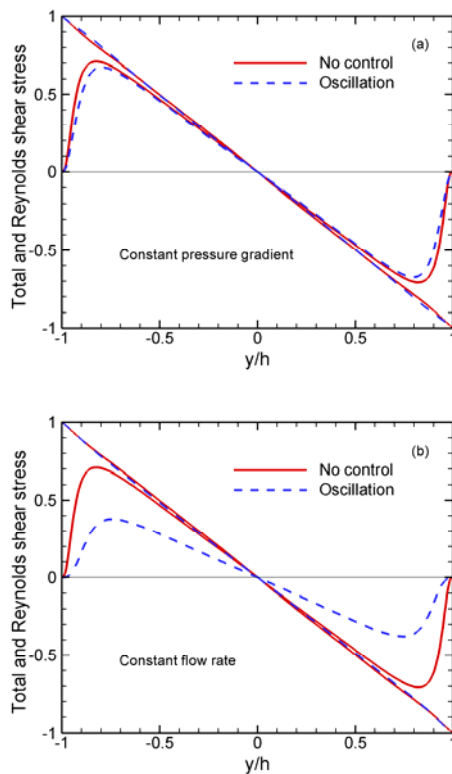

Figure 11. Reynolds and total shear stress in global coordinate: (a) Constant pressure gradient, (b) Constant flow rate.
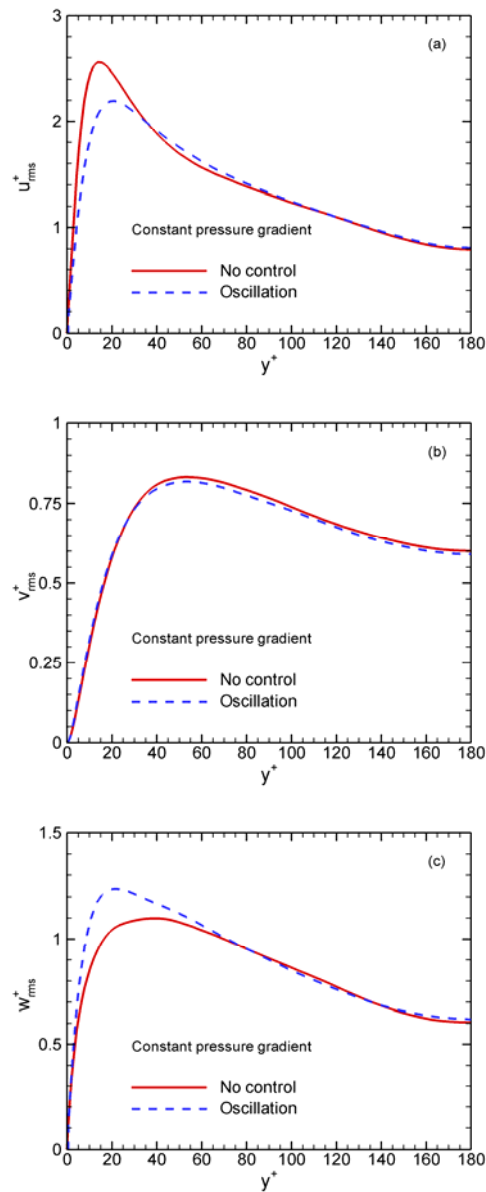
Figure 12. Profiles of root-mean-square velocity fluctuations with a constant pressure gradient in wall coordinate: (a) Streamwise, (b) Wall-normal, (c) Spanwise.

wall. The changes of turbulent intensities in the constant pressure gradient flow by the wall motion make a sharp contrast to those in the fixed mass flow. In the case of a constant mass flow, turbulence intensities are plotted in Figure 13 and all the turbulence intensities are found significantly reduced by the wall oscillation throughout the channel. For instance, approximately 27 % relative reduction in the streamwise intensity peak is
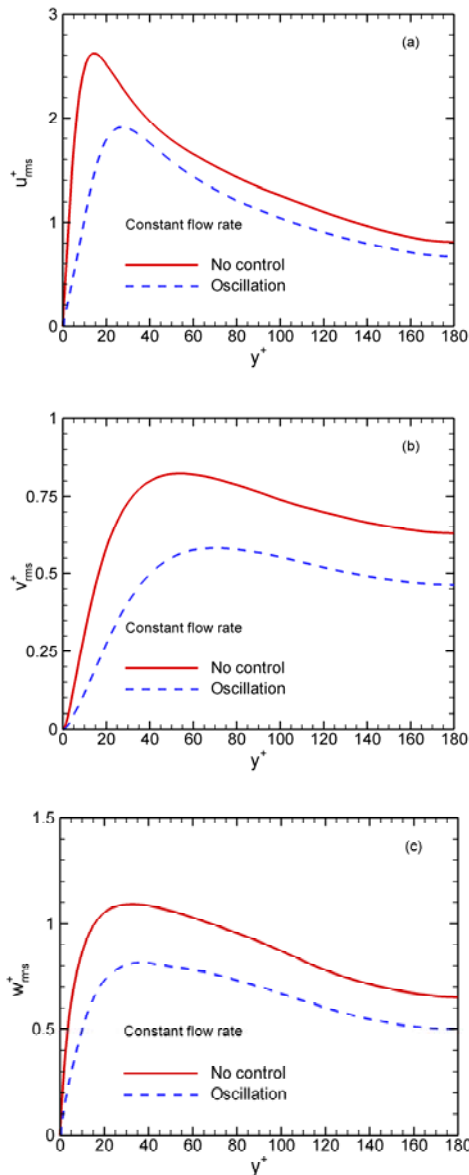
achieved. The outward shift of the peak streamwise turbulence intensity is apparent in both flow formulations, approximately 4 wall units from the wall for the constant pressure gradient flow and 10 wall units for the constant mass flow. The outward shift coincides respectively with the corresponding viscous sublayer thickness increase.

5.4. Production and Dissipation

Figure 14 shows the computed production ($-\rho \overline{u'v'} dU/dy$) and dissipation ($\mu \overline{\left(\partial u_i/\partial x_j\right)\left(\partial u_i/\partial x_j\right)}$) of the turbulent kinetic energy. In the case of a constant pressure gradient, it shows that the production peak is shifted toward the channel center and its peak value is also slightly increased by the wall motion. The maximum dissipation at the wall is found reduced by wall motions, with a more pronounced local maximum away from the wall. Again, the
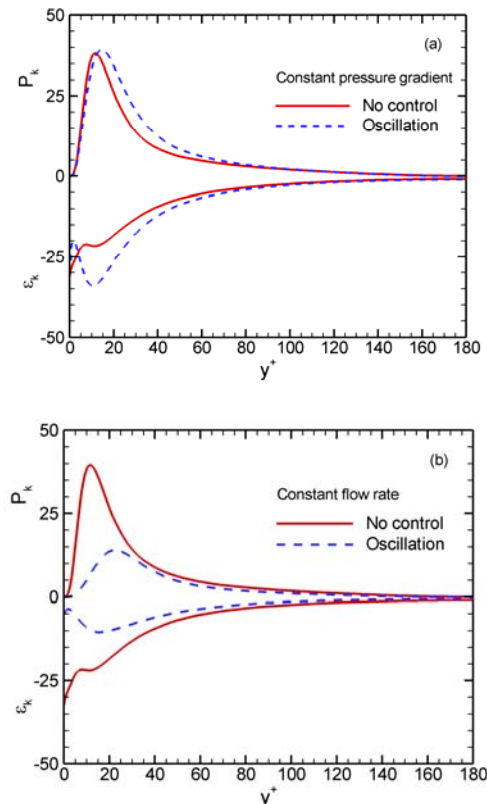
Figure 13. Profiles of root-mean-square velocity fluctuations with a constant flow rate in wall coordinate: (a) Streamwise, (b) Wall-normal, (c) Spanwise.

Figure 14. Profiles of production, dissipation in wall coordinate: (a) Constant pressure gradient, (b) Constant flow rate.

oscillation effect is confined to the near-wall region. Comparatively, the oscillation influence on the flow fields at a constant flow rate, as shown in Figure 14b, is throughout the entire channel. Not only the profiles of production and dissipation are shifted outwardly, but the reduction in their magnitudes is also more significant. However, in either case: constant flow rate or pressure gradient, the location of the production peak always corresponds to that of the maximum turbulence intensity in the streamwise direction.

5.5. Quadrant Analysis The quadrant analysis of the Reynolds shear stress provides the detailed information on the contributions from various events occurring in the flow to the total turbulence production [38]. The second-quadrant ($u' < 0$ and $v' > 0$), ejection events and the fourth-quadrant ($u' > 0$ and $v' < 0$), sweep events, contribute to the positive Reynolds shear stress $-\overline{u'v'}$. The first-quadrant ($u' > 0$ and $v' > 0$) and the third-quadrant ($u' < 0$ and $v' < 0$) events contribute to the negative Reynolds shear stress $-\overline{u'v'}$.

Figure 15 shows the contributions to the Reynolds shear stress from each quadrant. In the stationary channel (solid lines), the sweep event (fourth quadrant) is dominant in the wall region, while the ejection event (second quadrant) is dominant at locations away from the wall; these two contributions are about the same near $y^+ = 13$. This is true for both flow configurations. In the oscillating channel (dashed lines), if the pressure gradient is constant, Figure 15a shows that due to the wall motion, the contribution from ejections is reduced in the near-wall region but the contribution from sweeps is increased in its peak value. Despite the obvious alteration in the near-wall region, changes in either ejections or sweeps are less noticeable away from the wall. The Reynolds shear stress from the first and third quadrant events has little change. If the flow rate is constant, Figure 15b shows that both ejection and sweep events are substantially reduced by the wall motion throughout the entire channel. The Reynolds shear stress from the first and third quadrant events is also reduced by the wall oscillation. However, regardless of the wall motion, the sweep event is always dominant near the wall as seen in both flow formulations, although the location where the contributions from
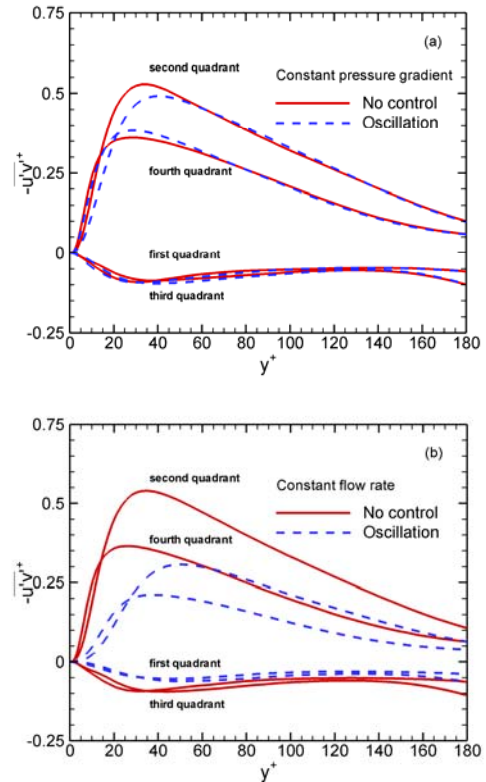

Figure 15. Reynolds shear stress from each quadrant: (a) Constant pressure gradient, (b) Constant flow rate.

ejection and sweep events are about the same is shifted by the wall motion from $y^+ \approx 13$ to $y^+ \approx 21$ in the constant pressure gradient flow but to $y^+ \approx 26$ in the fixed mass flow.

5.6. Vorticity Figures 16 and 17, respectively, show the root-mean-square vorticity fluctuations in the case of a constant pressure gradient and the case of a constant flow rate. Each vorticity component is denoted as ω_x, ω_y, ω_z in the streamwise, wall-normal and spanwise direction, respectively. In the stationary channel, the streamwise vorticity (ω_x) attains its maximum at walls with a local maximum further away from the wall. In the oscillating channel, the general distribution of streamwise vorticity (ω_x) is similar to that in the stationary channel. In the case of a constant pressure gradient, ω_x has much higher values as shown in Figure 16a, whereas in the case
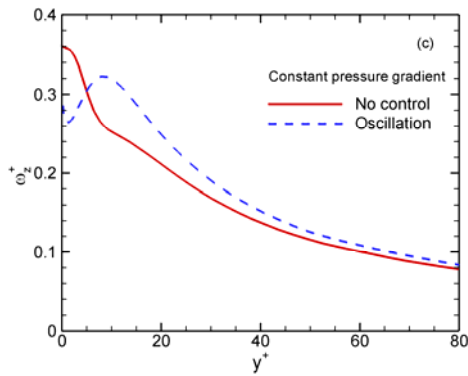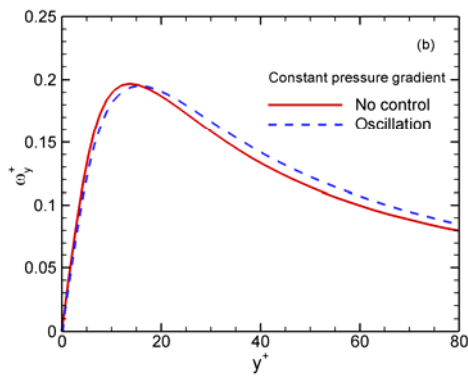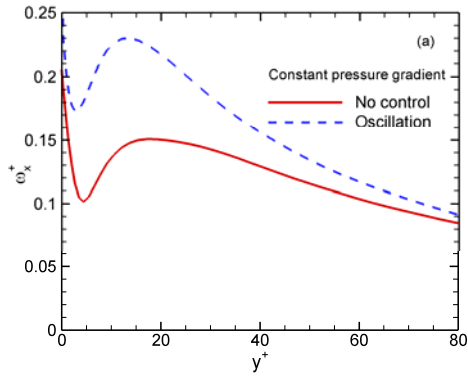
(ω_y) remains the same shape of profiles but is reduced significantly in the magnitude throughout the channel.

The spanwise vorticity components in Figures 16c and 17c are found altered significantly by the wall motion. In the stationary channel, they monotonically decrease from the maxima attained at the wall. In the oscillating channel however, both flows have a local maximum away from the
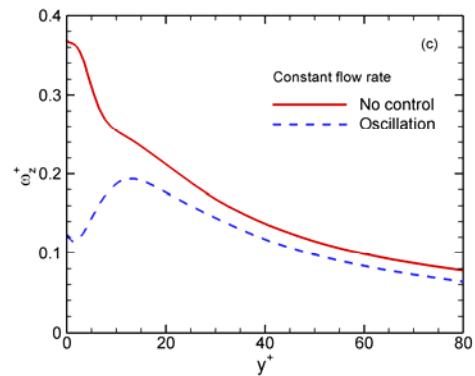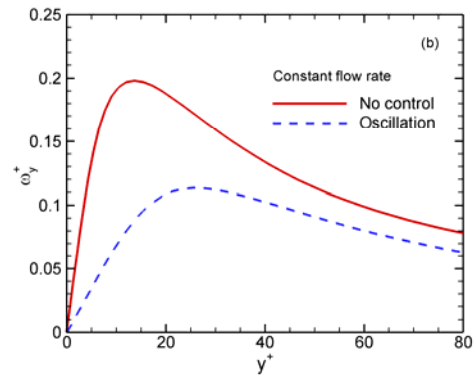
Figure 16. Profiles of root-mean-square vorticity fluctuations with a constant pressure gradient in near-wall region: (a) Streamwise, (b) Wall-normal, (c) Spanwise.

of a constant flow rate, ω_x has much lower values as shown in Figure 17a. The local positions of the streamwise vorticity peak, however, basically remain unchanged.

For the wall-normal vorticity (ω_y), the major difference is the outward shift of data with the wall oscillation for the case of a constant pressure gradient. For the case of a constant flow rate, Figure 17b shows that, the wall-normal vorticity
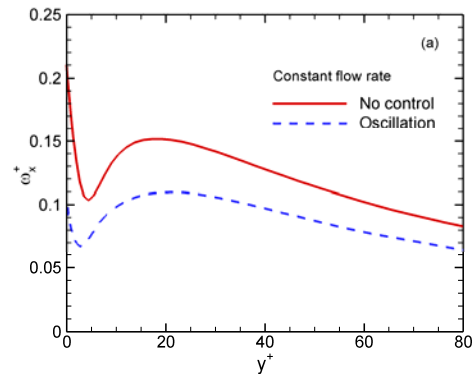
Figure 17. Profiles of root-mean-square vorticity fluctuations with a constant flow rate in near-wall region: (a) Streamwise, (b) Wall-normal, (c) Spanwise.

wall, approximately at $y^+ = 10$ in the case of a constant pressure gradient and at $y^+ = 14$ in the case of a constant flow rate. The outward shift of maximum spanwise vorticity (ω_z) is also displayed in both flows, with a more pronounced reduction in spanwise vorticity magnitude for the case of a constant flow rate. Similar observations for vorticity alteration by wall oscillations were also found by [2].

6. TURBULENCE INSTANTANEOUS FIELDS AND DISCUSSION

As shown in the previous section, turbulence statistics in the oscillating channel are significantly different from those in the stationary channel. Also, there exist differences between turbulence statistics for the constant pressure gradient flow and the constant flow rate flow. Their structures may have been altered differently by the wall motion. In this section, turbulence instantaneous flow fields will be examined.

In the case of a constant pressure gradient, the contour plots of streamwise velocity fluctuations in the (x-z) plane at various vertical positions are shown in Figure 18 for the stationary channel and in Figure 19 for the oscillating channel. In the case of a constant flow rate, they are plotted in Figures 20 and 21, respectively. The distinctive feature of the flow pattern in the stationary channel is the existence of highly elongated region of high speed ($u' > 0$) located adjacent to the low-speed ($u' < 0$) region in the vicinity of the wall, while they are absent in the region far away from the wall. This unique characteristic of the wall-layer turbulence is clearly seen at the near-wall region of $y^+ < 20$, whereas any definitely organized structures are absent in the computed flow patterns at the region far away from the wall.

In the oscillating channel, on the other hand, wall streaks in the constant pressure gradient flow in Figures 19a and 19b are still present in the regions of $y^+ = 6.5$ and $y^+ = 12$, but they are more weakened, broken and inclined with respect to the flow direction. The inclined streaks in the near-wall region are obviously attributed to the spanwise wall motion. In the case of a fixed mass flow rate, comparatively, the obvious modification
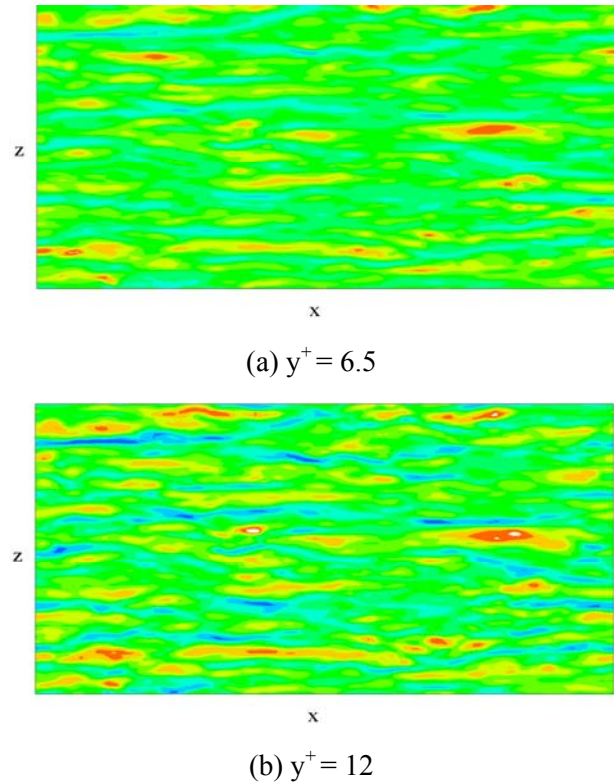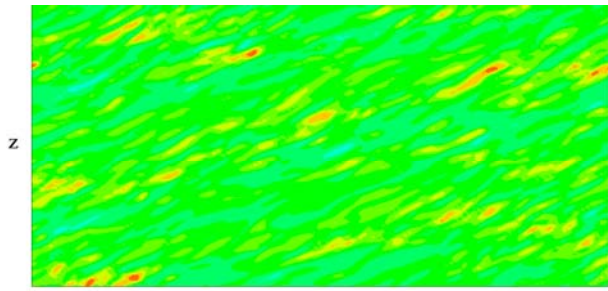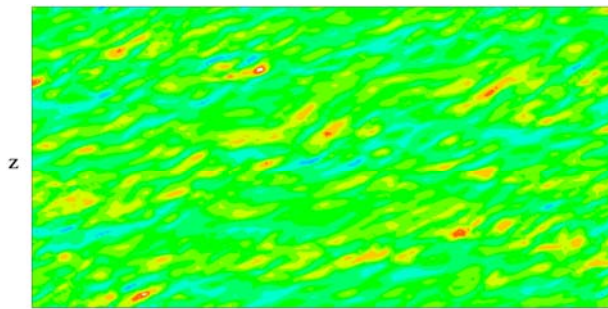

(a) $y^+ = 6.5$

(b) $y^+ = 12$

Figure 18. Contours of streamwise velocity fluctuations in a (x,z) plane in the case of a constant pressure gradient for a stationary channel.

of fundamental near-wall streaky structures in the oscillating channel is the reduced levels for most wall streaks in the region close to the wall as seen in Figure 21a for $y^+ = 6.5$ and in Figure 21b for $y^+ = 12$.

Figures 22 and 23 present the superposition of velocity vectors (v', w') and the contours of the streamwise vorticity fluctuation (ω_x) for both flow configurations. The structures with circular motions in the (y, z) plane and with large values of ω_x at the structure center, are identified as quasi-streamwise vortices. The circulation in the clockwise direction corresponds to the positive ω_x and those in the counterclockwise direction correspond to the negative ω_x. Most vortices in the stationary channel are observed in the buffer region ($10 < y^+ < 50$). In the immediate neighborhood of each positive ω_x, there is a corresponding counterpart of negative ω_x and vice versa, suggesting that the quasi-streamwise
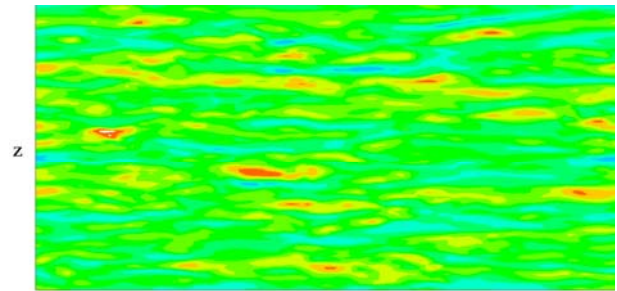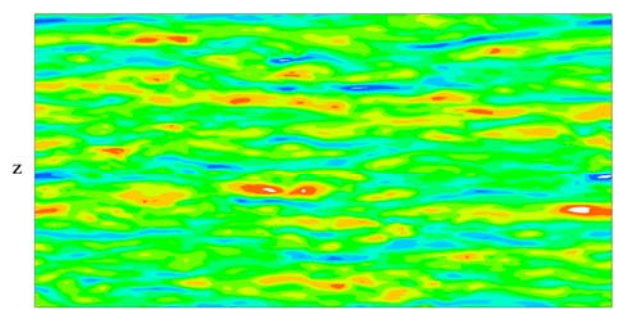
(a) $y^+ = 6.5$

(b) $y^+ = 12$

Figure 19. Contours of streamwise velocity fluctuations in a (x,z) plane in the case of a constant pressure gradient for an oscillating channel.

(a) $y^+ = 6.5$

(b) $y^+ = 12$

Figure 20. Contours of streamwise velocity fluctuations in a (x,z) plane in the case of a constant flow rate for a stationary channel.

structures might appear as counter-rotating pairs although their strengths might not be exactly the same.

In the oscillatory channels as shown in Figure 22b and 23b, turbulent activities in both cases are pushed away from the wall. At a constant flow rate, Figure 22b shows that streamwise vortices are still observed in the buffer region ($10 < y^+ < 50$) with substantially reduced strength. Besides, some vortices in the stationary channel do not appear at the same location in the oscillatory channel. The number of recognizable vortices is reduced from 12 in the stationary channel to 3 in the oscillating channel. Comparatively, streamwise vortices at a constant pressure gradient as shown in Figure 23b increased in strength, especially at the wall although the number of recognizable vortices does not appear to alter.

As to the mechanisms of drag reduction by the

wall oscillation, there is no doubt that the wall motion has interrupted the correlation between the streamwise vortices and the wall streaks. This study's numerical evidence, from the computed turbulence statistics and instantaneous flow fields, appears to support Trujillo's argument that it is the near-wall fluid and streaks which are shifted laterally, causing the disrupted coherence between the streaks and the streamwise vortices above the wall. If a flat plate is oscillated in a stationary fluid, because of viscous diffusion from plate surface, a thin boundary layer of shear flow, the Stokes layer, is formed over the plate. One of Stokes layer's effects is to push turbulence activities outward away from the wall. This has been seen in the distributions of streamwise velocity fluctuations (Figures 12a and 13a), turbulence production (Figure 14) and bursting events (Figure 15). In the case of a constant
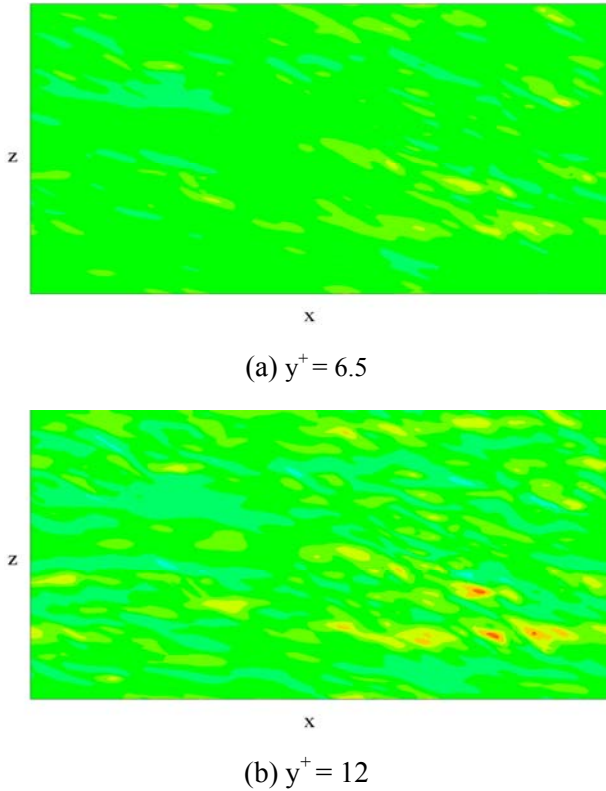
(a) $y^+ = 6.5$

(b) $y^+ = 12$

Figure 21. Contours of streamwise velocity fluctuations in a (x,z) plane in the case of a constant flow rate for an oscillating channel.

(a)

(b)

Figure 22. Superposition of velocity vectors and streamwise vorticity fluctuations in the (y,z) plane at x = 0 with the partial extent y/h = (-1.0 ~ -0.5) and full extent z/h = (0 ~ π) at a constant flow rate, (a) for a stationary channel, (b) in the oscillating channel.

(a)

(b)

Figure 23. Superposition of velocity vectors and streamwise vorticity fluctuations in the (y,z) plane at x = 0 with the partial extent y/h = (-1.0 ~ -0.5) and full extent z/h = (0 ~ π) at a constant pressure gradient, (a) for a stationary channel, (b) in the oscillating channel.

pressure gradient, wall streaks are also dragged in the spanwise direction through the Stokes layer in a sinuous pattern. This sinuous motion may place the streak under the influence of other preexisting vortices which may not be consistent with their original coherence. Furthermore, the streamwise vorticity of the wall seems to play a very important role in the wall-layer dynamics as well. As stated in the introduction, the wall streaks are responsible for generating streamwise vortices from an instability mechanism which is dominated by streamwise vorticity [36]. In order to overcome the distorted correlation of the streamwise vortex with the inclined wall-streaks, the streamwise vorticity at the wall as seen in Figures 16a and 23 has to be increased to reinforce its strength. This also explains why the velocity fluctuations are increased in the spanwise direction as presented in Figure 12c.
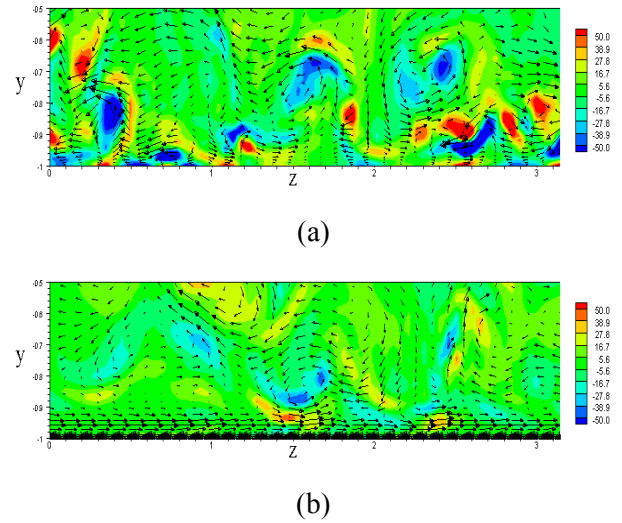
The scenario, however, for drag reduction in a

fixed mass flow by wall oscillation seems different when it is compared to that of the constant pressure gradient flow. First, throughout the entire channel,

the velocity, pressure and vorticity fluctuations, plus the Reynolds shear stress, are all substantially reduced by wall motions. The strength of near-wall streamwise vortices is also weakened. As a result, most of the high skin-friction regions are suppressed, leading to the drag reduction. Second, the most evident modification to the unperturbed channel data is the outward shift from the wall. This suggests that the high shear-rate region on the wall has moved towards the channel center, as seen in Figures 17c and 22. Consequently, the sweep (and ejection) events are significantly suppressed, resulting in drag reduction. Finally, the near-wall streaks at reduced levels no longer provide the source required for generating new streamwise vortices, which eventually slows down the turbulence self-sustaining process and thus less turbulence activity. In this sense, the wall oscillation has the effect of stabilizing wall streaks.

Streamwise vortical structures, comparatively, are less affected by the wall motion although their strength is altered. One argument, as suggested by [33], is that the average position of streamwise vortices is outside the Stokes layer. The other evidence which is also presented in Figures 16a and 17a is that, the positions of maximum streamwise vorticity fluctuation are less affected by wall motion, roughly at $y^+ \approx 18$, implying that the average position of streamwise vortical structures might not be altered. However, the upstream-end of the streamwise vortex located closer to the wall is found to follow the wall movement [33]. Further investigation into this argument needs to be carried out in the future.

7. SUMMARY

In this study, a fully developed turbulent channel flow subject to a spanwise wall oscillation has been simulated numerically via Fourier-Chebyshev-Tau spectral methods. Two flow configurations are examined: constant streamwise pressure gradient and constant streamwise flow rate. The skin-friction reduction is quantified by the change in wall-shear stress in the fixed mass flow or the change in flow rate in the constant pressure gradient flow. Although results produced in the stationary channel are identical for both flows, the transient process experienced in both flow configurations has resulted in different behaviors from each other.

Parametric study has shown more similarities between these two flow configurations as to the influence of the oscillation frequency, amplitude, orientation and Reynolds number upon the drag reduction, except for the optimal oscillation frequency, within $f^+ = 0.01\sim0.03$ for a constant pressure gradient and in between $f^+ = 0.005\sim0.02$ for a constant flow rate. When plotted as a function of the peak wall speed, drag reduction in the constant pressure gradient flow is increased with the increase in the peak wall speed, while for the fixed mass flow, drag reduction increases with the increasing peak wall speed initially and then it levels out, in agreement with experimental data. However, both flow configurations have comparable drag reduction percentage at the range of peak wall speed $W_p^+ \leq 20$, with the maximum value of 42 %.

Despite the large magnitude of drag reduction, the amount of energy input which is required to produce the desired drag reduction is also significant. Only a small net gain of about 5% was obtained. The spanwise wall oscillation does not seem to be economically practical for the turbulent flow configurations studied, in which the entire wall is put into motion.

The statistics for the oscillating channel are compared to those in the stationary channel for both flow formulations. The most evident modification by the wall oscillation is the outward shift in the data set with wall oscillation. In the case of a constant pressure gradient, some turbulent quantities are increased but others are decreased. This variation of turbulent statistics with wall oscillation is in sharp contrast to the results for the oscillating channel flow at a fixed flow rate, in which all the turbulent quantities such as the velocity, pressure and vorticity fluctuations are significantly reduced throughout the channel.

Instantaneous flow fields show that the near-wall flow structures have been altered differently by wall oscillations for the constant pressure gradient flow and the constant mass flow. However, numerical evidence presented here supports such an argument that it is the near-wall fluid and streaky structures that have been altered and in turn they are responsible for the drag reduction by the wall motion.

8. ACKNOWLEDGEMENTS

9. NOMENCLATURE

C_f	Skin-Friction Coefficient = $\tau_w/(\rho U^2/2)$
f, T	Oscillation Frequency and Period, T = 1/f
h	Channel Half-Width
k	Turbulence Kinetic Energy
Q	Volumetric Flow Rate Per Unit Width = 2hU
p, P	pressure and Mean Pressure
$P_{k, \varepsilon}$	production and Dissipation Rate of k
Re_m	Reynolds Number = $2hU/\nu$
Re_Q	Reynolds Number = $3Q/4\nu$
Re_P	Reynolds Number = $-(dP/dx) \bullet h3 / (2\rho\nu^2)$
Re_τ	Reynolds Number = $u_\tau h/\nu$
t	Time
U	Bulk Mean Velocity
u_τ	Wall-Shear Velocity = $(\tau_w/\rho)^{1/2}$
u, v, w	Velocity Components in the x, y and z Direction
W_a	Velocity Amplitude of Wall Oscillation
W_p	Peak Wall Speed = $(\Delta z/2)\bullet(2\pi f)$
x_i	Coordinate in the ith Direction; x_1, x_2 and x_3 Denotes x, y and z, Respectively
Δz	Peak-to-Peak Amplitude in the Spanwise Direction Within on Period
γ	Oscillation Orientation Measured With Respect to the Mean Flow (Streamwise) Direction
δ	Viscous Penetrating Boundary Layer Thickness
ρ, ν	Density and Kinematic Viscosity
$\omega_x, \omega_y, \omega_z$	Vorticity in the x, y and z Direction, Respectively
τ_w	Streamwise Wall-Shear Stress, = $\mu dU/dy$
τ_{wz}	Streamwise Wall-Shear Stress, = $\mu(\overline{dw'/dy})$

Superscripts and Subscripts

( )'	Fluctuating Component
( )$^+$	Normalized by the Wall Variables u_τ and ν
$\overline{(\ )}$	Ensemble Average Over the x-z Plane and Time
( )$_{rms}$	Root-Mean-Square Value
( )$_0$	Value in the Free Case
( )$_{osci}$	Value in the Forced Case
( )$_w$	Value at Walls
< >	Ensemble Average Over the x-z Plane

10. REFERENCES

1. Robinson, S. K., "Coherent Motions in the Turbulent Boundary Layer", *Annu. Rev. Fluid Mech.*, Vol. 23, (1991), 601-639.
2. Baron, A. and Quadrio, M., "Turbulent Drag Reduced by Spanwise Wall Oscillations", *Appl. Sci. Research*, Vol. 55, (1996), 311-326.
3. Choi, K. S., "Near-Wall Structure of Turbulent Boundary Layer with Spanwise-Wall Oscillation", *Phys. Fluids*, Vol. 4, No.7, (2002), 2530-2542.
4. Quadrio, M. and Ricco, P., "Critical Assessment of Turbulent Drag Reduction through Spanwise Wall Oscillation", *J. Fluid Mech.*, Vol. 521, (2004), 251-271.
5. Zhou, D. M. and Ball, K. S., "Effects of Spatial Resolution and Box Size on Numerical Solutions of Turbulent Flow", *ASME Fluids Engineering Summer Conference*, Houston, TX, (June 19-23, 2005).
6. Laadhari, F., Skandaji, L. and Morel, R., "Turbulence Reduction in a Boundary Layer by a Local Spanwise Oscillating Surface", *Phys. Fluids*, Vol. 6, No. 10, (1994), 3218-3220.
7. Choi, K. S., DeBisschop, J. R. and Clayton, B. R., "Turbulent Boundary-Layer Control by Means of Spanwise-Wall Oscillation", *AIAA J.*, Vol. 36, No. 7, (1998), 1157-1163.
8. Choi, K. S. and Graham, M., "Drag Reduction of Turbulent Pipe Flows by Circular-Wall Oscillation", *Phys. Fluids*, Vol. 10, (1998), 7-9.
9. Trujillo, S. M., Bogard, D. G. and Ball, K. S., "Turbulent Boundary Layer Drag Reduction Using an Oscillating Wall", *28th AIAA Fluid Dynamics*

Conference, 4th AIAA Shear Flow Control Conference, Snowmass Village, CO, (June 29-July 2, 1997).

10. Trujillo, S. M., "An Investigation of the Effects of Spanwise Wall Oscillation on the Structure of a Turbulent Boundary Layer", Ph.D. Dissertation, The Univ. of Texas at Austin, (1999).

11. Wu, S. L., "An Investigation of the Reynolds Number Effect on the Drag Reduction by Spanwise Wall Oscillation", Master Thesis, The Univ. of Texas at Austin, (2000).

12. Di Cicca, G. M., Iuso, G., Spazzini, P. G. and Onorato, M., "Particle Image Velocimetry Investigation of a Turbulent Boundary Layer manipulated by Spanwise Wall Oscillations", *J. Fluid Mech*., Vol. 467, (2002), 41-56.

13. Quadrio, M. and Sibilla, S., "Numerical Simulation of Turbulent Flow in a Pipe Oscillating Around its Axis", *J. Fluid Mech*., Vol. 424, (2000), 217-241.

14. Du, Y., Symeonidis, V. and Karniadakis, G. E., "Drag Reduction in Wall-Bounded Turbulence via a Transverse Traveling Wave", *J. Fluid Mech*., Vol. 457, (2002), 1-34.

15. Zhao, H., Wu, J. Z. and Luo, J. S., "Turbulent Drag Reduction by Traveling Wave of Flexible Wall", *J. Fluid Dynamics Research*, Vol. 34, (2004), 175-198.

16. Robinson, S. K., "Coherent Motions in the Turbulent Boundary Layer", *Annu. Rev. Fluid Mech*., Vol. 23, (1991), 601-639.

17. Kravchenko, A. G., Choi, H. and Moin, P., "On the Relation of Near-Wall Streamwise Vortices to Wall Skin Friction in Turbulent Boundary Layers", *Phys. Fluids A*., Vol. 5, No. 12, (1993), 3307-3309.

18. Bernard, P. S., Thomas, J. M. and Handler, R. A., "Vortex Dynamics and the Production of Reynolds Stress", *J. of Fluid Mech*., Vol. 253, (1993), 385-419

19. Brooke, J. W. and Hanratty, T. J., "Origin of Turbulence-Producing Eddies in a Channel Flow", *Phys. Fluids A*., Vol. 5, (1993), 1011-1022.

20. Choi, H., Moin, P. and Kim, J., "Direct Numerical Simulation of Turbulent Flow over Riblets", *J. Fluid Mech*., Vol. 255, (1993), 503-539.

21. Orlandi, P. and Jimenez, J., "On the Generation of Turbulent Wall Friction", *Phys. Fluids*, Vol. 6, No. 2, (1994), 634-641.

22. Jimenez, J. and Pinelli, A., "The Autonomous Cycle of Near-Wall Turbulence," *J. Fluid Mech*., Vol. 389, (1999), 335-359.

23. Kim, J., Moin, P. and Moser, R., "Turbulence Statistics in Fully Developed Channel Flow at Low Reynolds Number", *J. Fluid Mech*., Vol. 177, (1987), 133-166.

24. Schoppa, W. and Hussain, F., "Coherent Structure Dynamics in Near-Wall Turbulence", *J. Fluid Dynamics Research*, Vol. 34, (2000), 175-198.

25. Miyake, Y., Tsujimoto, K. and Takahashi, M., "On the Mechanism of Drag Reduction of Near-Wall Turbulence by Wall Oscillation", *JSME Inter. J. Series B*., Vol. 40, No. 4, (1997), 558-566.

26. Dhanak, M. R. and Si, C., "On Reduction of Turbulent Wall Friction through Spanwise all Oscillation", *J. Fluid Mech*., Vol. 383, (1999), 175-195.

27. Choi, K. S. and Clayton, B. R., "The Mechanism of Turbulent Drag Reduction with Wall Oscillation," Inter. J. of Heat and Fluid Flow, Vol. 22, (2001), 1-9.

28. Karniadakis, G. E. and Choi, K. S., "Mechanisms on Transverse Motions in Turbulent Wall Flows", *Annu. Rev. Fluid Mech*., Vol. 35, (2003), 45-62.

29. Moin, P. and Mahesh, K., "Direct Numerical Simulation: A Tool in Turbulence Research", *Annu. Rev. Fluid Mech*., Vol. 23, (1998), 601-639.

30. Rozhdestvensky, B. L. and Simakin, I. N., "Secondary Flows in a Plane Channel: Their Relationship and Comparison with Turbulent Flows", *J. Fluid Mech*., Vol. 147, (1984), 261-289.

31. Jimenez, J., "Transition to Turbulence in Two-Dimensional Poiseuille Flow", *J. Fluid Mech*., Vol. 218, (1990), 265-297.

32. Canuto, C., Hussaini, M. Y., Quarteroni, A. and Zang, T. A., "Spectral Methods in Fluid Dynamics", Springer-Verlag, New York, (1988).

33. Zhou, D.-M., "A Direct Numerical Simulation of Fully Developed Turbulent Channel Flow with Spanwise Wall Oscillation", Ph.D. Dissertation, The Univ. of Texas at Austin, (2005).

34. Del Alamo, J. C. and Jimenez, J., "Spectra of the Very Large Anisotropic Scales in Turbulent Channels", *Phys. Fluids*, Vol. 15, No. 6, (2003), L41-L44.

35. Dean R. B., "Reynolds Number Dependence of Skin Friction and Other Bulk Flow Variables in Two-Dimensional Rectangular Duct Flow", *Trans. ASME I: J. Fluid Eng*., Vol. 100, (1978), 215-223.

36. Choi, H., Moin, P. and Kim, J., "Active Turbulence Control for Drag Reduction in Wall-Bounded Flows", *J. Fluid Mech*., Vol. 262, (1994), 75-110.

37. Tardu S. F., Binder, G. and Blackwelder, R. F., "Turbulent Channel Flow with Large-Amplitude Velocity Oscillation", *J. Fluid Mech*., Vol. 267, (1994), 109-151.

38. Lu, S. S. and Willmarth, W. W., "Measurements of the Structure of the Reynolds Stress in a Turbulent Boundary Layer", *J. Fluid Mech*., Vol. 60, (1973), 481-511.

39. Berger, T. W., Kim, J., Lee, C. and Lim, J., "Turbulent Boundary Layer Control Utilizing the Lorentz Force", *Phys. Fluids*, Vol. 12, No. 3, (2000), 631-649.

40. Choi, J. I., Xu, C. X. and Sung, H. J., "Drag Reduction by Spanwise Wall Oscillation in Wall-Bounded Turbulent Flows", *AIAA J*., Vol. 40, No. 5, (2002), 842-850.

41. Gad-el-Hak, M., "Flow Control: Passive, Active and Reactive Flow Management", Cambridge University Press, New York, U.S.A., (2000).

42. Kim, J., "Control of Turbulence Boundary Layers", *Phys. Fluids*, Vol. 15, No. 5, (2003), 1093-1105.

43. Moin, P., Shih, T. H., Driver, D. and Mansour, N. N., "Direct Numerical Simulation of a Three-Dimensional Turbulent Boundary Layer", *Phys. Fluids A*., Vol. 2, No. 10, (1990), 1846-1853.